Vacancy-induced dissolution of precipitates in out-of-equilibrium systems: A test case of FeX (X=C,N,O) alloys

Thomas Schuler*
Department of Materials Science and Engineering, University of Illinois, Urbana-Champaign, Illinois 61801, USA and DEN-Service de Recherches de Métallurgie Physique, CEA, Université Paris-Saclay, F-91191, Gif-sur-Yvette, France

Maylise Nastar and Frédéric Soisson
DEN-Service de Recherches de Métallurgie Physique, CEA, Université Paris-Saclay, F-91191, Gif-sur-Yvette, France
(Received 24 September 2016; revised manuscript received 21 November 2016; published 30 January 2017)

Various out-of-equilibrium processes produce a supersaturation of vacancies in the material. When these defects show attractive binding energy with solutes, they will form stable point defect-solute clusters which will stabilize solutes in the solid solution with respect to the equilibrium case. Hence the out-of-equilibrium dynamic solubility limit increases, which can lead to the dissociation of solute precipitates. This vacancy-induced precipitate (VID) dissolution mechanism is an alternative to the well-known ballistic mixing effect (BAL) under irradiation, and it is also relevant for quenching, ball milling, and severe plastic deformation. Under irradiation, a BAL is efficient at low temperature only, whereas a VID is expected to be effective at intermediate temperatures. A quantitative and consistent prediction of the interstitial solute solubility limit increase generated by both BAL and VID mechanisms is presented starting from *ab initio* binding energies and migration energies of solutes and point defects, and using a low-temperature expansion of the free energy of the solid solution. These results are discussed for three alloys: FeC, FeN, and FeO, the latter being relevant to discuss the stability of oxide dispersed strengthened alloys microstructure under irradiation. We also suggest an experiment that would be able to determine steady-state vacancy supersaturations from the measure of solute partial pressures in out-of-equilibrium systems.

DOI: 10.1103/PhysRevB.95.014113

I. INTRODUCTION

Most materials processing routes consist in driving a system out of equilibrium to reach a particular microstructure related to the desired properties. These systems are then kinetically trapped in a metastable state from which it is difficult to escape, hence the durability of the materials properties. When the external force that drives the system out-of-equilibrium is sustained (irradiation, ball milling, severe plastic deformation), the usual thermodynamic phase diagram becomes a dynamic phase diagram, where the steady state, or dynamic equilibrium, is a function of both thermodynamic and kinetic properties of the system, as well as these external driving forces [1–9].

Materials under irradiation offer many examples of such dynamic equilibrium, based on various mechanisms. The first mechanism is denoted as ballistic mixing, which can cause precipitate dissolution (or resolution) and patterning (precipitation with a given precipitate length scale [7,9]). The highly energetic incident neutron particle transfers enough energy to an atom to kick it out of its location, thus creating a Frenkel pair [vacancy V + self-interstitial atom (SIA)]. Consider a two-phase equilibrium (solid solution + precipitate): if the primary knock-on atom was located inside a precipitate, there is a certain probability that it will be ejected from this precipitate and end up in the solid solution. The reverse is also true, an atom belonging to the solid solution can also be displaced toward a precipitate. The atom in solution will then diffuse and associate with a precipitate, or form new precipitates over a diffusion time scale. Depending on the combination of various irradiation parameters such as the nature and energy of incident particles, irradiation flux, temperature, microstructure, etc., there are three possible steady-state microstructures [7]: (1) a random solid solution; (2) binary equilibrium between the solid solution and the precipitated phase (where the solubility limit may be higher than the equilibrium one); (3) a steady state where both the solid solution and finite-size precipitates exist, also called patterning regime. As an example, the stability of the microstructure of oxide-dispersed strengthened (ODS) alloys under irradiation is key to the sustainability of their mechanical properties and their safe use as structural and cladding materials in future nuclear reactors [10,11]. Nevertheless, classical ballistic mixing models do not seem to quantitatively account for the observed dissolution of ODS particles under irradiation at relatively high temperatures [12–14], while there seems to be a qualitative agreement for samples irradiated at room temperature [15]. Other mechanisms have been put forward to explain the contradictory data on ODS particle stability under irradiation (see, e.g., Ref. [16] for a review): vacancy flux and solute drag effect [17], balance between ballistic mixing and radiation-enhanced diffusion [16,18], interface coherency effect [19,20]. While all of these effects might be happening simultaneously, it is still unclear which factors control the ODS particle size and density under irradiation. Also note that radiation-enhanced diffusion is not applicable to interstitial solutes like oxygen because they are able to diffuse on their own, and a large concentration of point defects would be necessary to significantly modify the average solute diffusivity.

Another mechanism of dynamic equilibrium is due to the attractive interaction between solutes and point defects (V and SIA). Defects are produced in excess under irradiation,

*Corresponding author: tschul@illinois.edu

so there is a driving force for them to eliminate at point defect sinks. During the course of their diffusion to sinks, they might encounter solute atoms and contribute to their transport [21–24] and redistribution. Depending on the details of the thermodynamic and kinetic interaction between point defects and solutes, it can lead to radiation-induced segregation at point defect sinks [25–28] and radiation-induced precipitation, both heterogeneous [29,30] and homogeneous [31].

It has been shown in previous studies that despite the low concentration of V under equilibrium condition, these defects already contribute to the solubility limit of oxygen in a ferrite solid solution [32]. Also, low concentrations of interstitial solutes stabilize many vacancies in the solid solution, and reduce the effective vacancy formation energy in the system [33]. In both cases, vacancies and interstitial solutes have a highly attractive binding energy, and because of that they stabilize each other in the solid solution. Under out-of-equilibrium steady-state conditions, the same mechanism operates, except that the vacancy concentration is imposed by some external driving force. Mathematically, the problem of solute phase boundary shift can be solved in the framework of constrained thermodynamics [1,4] because local equilibrium can be assumed on a small volume of the material [5]. Earlier work using the concept of constrained thermodynamics [1,4] conclude that a large concentration of point defects is required to shift phase boundaries significantly, because they consider that each point defect increases the energy of the phase by an amount equal to the point defect formation energy. This conclusion is based on an oversimplified description of the effect of point defects on the phase diagram. For example, the results from Ref. [32] show that large vacancy concentrations are not necessary to change the solubility limit for an equilibrium between a solid solution and a precipitate of interstitial solutes, because the solute concentration in both phases differs by orders of magnitude and the vacancy-solute interaction can be very attractive. Moreover, previous models did not consider the coupling between the thermodynamic and kinetic interplay of vacancies and solutes: solute solubility limits depend on the concentration of point defects, which themselves depend on the kinetic average properties of point defects, hence on solute solubility limits. This coupling requires a detailed and consistent modeling of both the thermodynamic and diffusion properties of the system.

The goal of this paper is to provide a general and quantitative methodology to compute the effect of both ballistic mixing and vacancy-induced dissolution mechanisms in a unified framework and identify the temperature/irradiation flux region where each mechanism is most effective. Predictions of solute-point defect thermodynamic and kinetic properties and the solid solution/precipitate phase boundary shift in steady-state out-of-equilibrium alloys are based on atomic scale data computed from *ab initio*. We restrict this study to the effect of vacancies and assume no interaction between solutes and SIA. Section II presents the methods (low-temperature expansion of the free energy based on *ab initio* data), and Sec. III introduces the parameters used in our models for FeC, FeN, and FeO solid solutions. In Sec. IV, the solubility limit increase of solutes as a function of vacancy supersaturation is obtained for three systems: FeC, FeN, and FeO (Sec. IV A). A ballistic mixing model is derived for interstitial solutes, which do not show radiation-enhanced diffusion and we provide an assessment of the BAL and VID domains for the FeO system (Sec. IV B). Finally, Sec. V presents potential applications of these calculations: using a very simplified model for ODS materials, our calculations display some features that are in qualitative agreement with experimental observations of radiation-induced precipitate dissolution (Sec. V A); we also suggest a new experimental protocol for measuring out-of-equilibrium vacancy concentrations from solute partial pressures (Sec. V B).

II. DYNAMICAL PHASE DIAGRAM FROM LTE FREE ENERGIES

Low-temperature expansion (LTE [32,34–40]) is a powerful technique to compute equilibrium properties of alloys. A reference state is chosen for the system, and then a series of excitation states are considered, sorted by their energy with respect to the reference system. If the latter is correctly chosen as the most energetically favored state, then at 0 K temperature, it is the only possible state. As temperature increases, more and more excitation states have non-negligible probability. The idea of LTE is to expand the partition function of the system around the reference state, and to derive the approximate free energy of the system from this truncated partition function. Then, all thermodynamic properties are obtained from this analytical expression of the LTE free energy, for instance, cluster size distributions [40], phase diagrams [36], and interface defects [39]. Despite its name, LTE may give reliable results up to fairly high temperatures depending on the energies of the excited states (at least 1100 K for C, N, and O in Fe because of high binding energies with vacancies [32]). For completeness, we derive below the LTE expression of the free energy in the grand-canonical ensemble, and the equation one has to solve to compute the equilibrium chemical potential between two phases in multi-component alloys.

In the grand-canonical ensemble, the grand potential of the system $\mathcal{A}$ is a function of the grand-canonical partition function Ξ:

$$\mathcal{A} = -k_B T \ln(\Xi), \tag{1}$$

where T denotes the temperature, k_B denotes the Boltzmann constant, and Ξ reads

$$\Xi = \sum_i \exp\left[\frac{-E_i + \sum_\alpha n_\alpha(i)\mu_\alpha}{k_B T}\right]. \tag{2}$$

The sum runs over every state i of the system, having energy E_i and containing $n_\alpha(i)$ particles of species α, to which is associated the chemical potential μ_α. The reference state chosen for the system has energy E_0 and contains $n_\alpha(0)$ particles of each species α. Now, the partition function is factorized by the term corresponding to the reference state, and the grand-potential reads

$$\mathcal{A} = \left(E_0 - \sum_\alpha n_\alpha(0)\mu_\alpha\right) - k_B T \ln\left[1 + \sum_i G_{\zeta_i} \exp\left(\frac{\zeta_i}{k_B T}\right)\right], \tag{3}$$

with

$$\zeta_i = -(E_i - E_0) + \sum_\alpha (n_\alpha(i) - n_\alpha(0))\mu_\alpha$$
$$= -\Delta E_i + \sum_\alpha \Delta n_\alpha(i)\mu_\alpha. \quad (4)$$

The sum over all states i in Eq. (3) runs over states for which $\zeta_i < 0$ only (if not, then the reference state has not been chosen properly as there exists at least one more stable state). These configurations ($\zeta_i < 0$) are called excited states. These can be sorted by their ζ_i values, and G_{ζ_i} denotes the degeneracy (number of equivalent states) of configuration ζ_i. We then set a value ζ_M such that any states which verifies $\zeta_i > \zeta_M$ has a negligible influence on the thermodynamic properties of the system at the temperature of interest. At low temperature, i.e., $\sum_i \exp[\frac{\zeta_i}{k_B T}] \ll 1$, the logarithm function in Eq. (3) can be expanded to first order:

$$\mathcal{A} = \mathcal{A}_0 - k_B T \sum_{0<\zeta_i\leqslant\zeta_M} G_{\zeta_i} \exp\left(\frac{\zeta_i}{k_B T}\right), \quad (5)$$

where $\mathcal{A}_0 = E_0 - \sum_\alpha n_\alpha(0)\mu_\alpha$ is the grand-potential of the reference state. The concentration per lattice site (N_s lattice sites in the system) is then obtained from Eq. (5):

$$[\alpha] = -\frac{1}{N_s}\frac{\partial \mathcal{A}}{\partial \mu_\alpha}$$
$$= \frac{n_\alpha(0)}{N_s} + \sum_{0<\zeta_i\leqslant\zeta_M} n_\alpha(\zeta_i) P_{\zeta_i}, \quad (6)$$

where the probability P_{ζ_i} of each excited state ζ_i is

$$P_{\zeta_i} = g_{\zeta_i} \exp\left[\frac{-\Delta E_{\zeta_i} + \sum_\alpha \Delta n_\alpha(\zeta_i)\mu_\alpha}{k_B T}\right], \quad (7)$$

and $g_{\zeta_i} = G_{\zeta_i}/N_s$ is interpreted as the exponential of the configurational entropy of this excited state.

To obtain equilibrium chemical potentials between two phases, one needs to perform the LTE [Eq. (5)] for each of the two phases independently (each one has a different reference state), and then use the equilibrium condition, that is, the equality of grand-potentials. If there are more than one independent chemical potential in the system, the other ones are found either considering other phases in equilibrium or treating the corresponding species in the canonical ensemble (fixed concentration) and using Eq. (6) to compute the chemical potential.

Following this general presentation of LTE, we now introduce the specific features of this paper. We aim at investigating the effect of irradiation on the solubility limit of interstitial impurities (C, N, and O) in α-Fe. Note that this calculation of cluster concentrations is an equilibrium calculation *per se*, but these relations are assumed to hold when the system is driven out of equilibrium. This is the local equilibrium assumption, which states that the local evolution of the system is fast enough to reach a constrained equilibrium state at each time. This assumption is thus likely to fail at low temperature and high irradiation flux.

Point defects are created under irradiation, and diffuse, recombine and eliminate at point defect sinks. It is known that after some time, a steady-state concentration profile of point defects in the solid solution is reached [8]. In this paper, we focus on the interaction between vacancies and solute impurities. As a simplifying assumption, interactions between self-interstitial atoms and solutes are neglected and the effect of irradiation will be approximately modeled by a steady-state vacancy supersaturation (although self-interstitial atoms will be considered in our rate theory model to compute the steady-state vacancy supersaturation for a given temperature and irradiation flux). Simple analytical expressions from rate theory provide estimates of vacancy supersaturation as a function of irradiation and microstructure parameters [8]. On the other hand, it has been shown that under equilibrium conditions where vacancy concentrations are very low, vacancies need to be accounted for in the calculation of the equilibrium solubility limit, especially for the Fe-O alloy [32]. In the present work, we investigate the effect of a steady-state out-of-equilibrium vacancy concentration on solute solubility limits. Because the steady-state vacancy concentration profile does not evolve with time, vacancies will be treated as conservative species (canonical ensemble).

The solubility limit is obtained considering the equilibrium between the solid solution (containing interstitial species C, N, and O) and some ordered structure of these solutes in Fe (carbide Fe_3C, nitride Fe_4N, or oxide FeO and Fe_3O_4, respectively). In order to simplify the parametrization of our model, we choose to describe in fine details the free energy of the solid solution (especially how it varies with interstitial solutes and vacancy concentrations) and to adopt a semi-phenomenological approach to estimate the free energy of the solute ordered phase (assumed perfectly stoechiometric), as explained in Ref. [32]. Ignoring the excited states of the ordered phase (insertion of vacancies and/or antisites) is justified by the following reasoning: the equilibrium chemical potential of a solute is related to the difference between the average solute formation energy in each phase, the solid solution and the ordered compound; the solute concentration in the solid solution being very low, the average solute formation energy is easily altered when some of the solutes are close to vacancies, with which they show attractive binding; in the ordered phase containing 25%–50% solutes, concentration of defects of the same order of magnitude would be needed to significantly alter the average solute formation energy in this phase. If such a high defect concentration existed in the ordered phase, these defects should most probably exist in the ground state configuration of this phase, which means that the reference state for this phase has been badly chosen.

With that in mind, let $\mathcal{A}(Fe_pX_q)$ be the grand-potential per Fe atom of the ordered compound:

$$\mathcal{A}(Fe_pX_q) = \frac{\Delta\mathcal{F}(Fe_pX_q)}{p} - \mu_{Fe} - \frac{q}{p}\mu_X. \quad (8)$$

In this work, chemical potentials are expressed with respect to the isolated atom/defect in otherwise perfect bulk α-Fe. With these references, the energy difference between the ordered

compound and bulk α-Fe is

$$\begin{aligned}\frac{\Delta\mathcal{F}(\mathrm{Fe}_p X_q)}{p} &= \frac{\mathcal{F}_{[\mathrm{Fe}_p X_q]}}{p} - \frac{\mathcal{F}_{[N_{\mathrm{Fe}}\mathrm{Fe}]}}{N_{\mathrm{Fe}}} - \frac{q}{p}\left(\mathcal{F}_{[N_{\mathrm{Fe}}\mathrm{Fe}+X]} - \mathcal{F}_{[N_{\mathrm{Fe}}\mathrm{Fe}]}\right)\\ &= -\frac{q}{p}\left(\mathcal{F}_{[N_{\mathrm{Fe}}\mathrm{Fe}+X]} - \mathcal{F}_{[\mathrm{Fe}_{p/q}X]} - \mathcal{F}_{[N_{\mathrm{Fe}}\mathrm{Fe}]} + \frac{p}{q}\frac{\mathcal{F}_{[N_{\mathrm{Fe}}\mathrm{Fe}]}}{N_{\mathrm{Fe}}}\right)\\ &= -\frac{q}{p}\left(\mathcal{F}_{[N_{\mathrm{Fe}}\mathrm{Fe}+X]} - \mathcal{F}_{[\mathrm{Fe}_{p/q}X]} - \mathcal{F}_{\left[\left(N_{\mathrm{Fe}}-\frac{p}{q}\right)\mathrm{Fe}\right]}\right)\\ &= -\frac{q}{p}\mathcal{F}^f(X)_{|\mathrm{Fe}/\mathrm{Fe}_p X_q}. \end{aligned} \tag{9}$$

$\mathcal{F}_{[\Theta]}$ is the total free energy of a supercell containing Θ. $\mathcal{F}^f(X)_{|\mathrm{Fe}/\mathrm{Fe}_p X_q}$ [later denoted simply by $\mathcal{F}^f(X)$] is defined as the solute formation free energy in α-Fe, the reference solute state being the ordered phase $\mathrm{Fe}_p X_q$.

If two phases are at equilibrium, their grand potentials must be equal,

$$-\frac{q}{p}\mathcal{F}^f(X) - \mu_{Fe} - \frac{q}{p}\mu_X = -\mu_{Fe} - k_B T\sum_{\zeta_i} P_{\zeta_i}, \tag{10}$$

which is rewritten in a more convenient form:

$$\frac{q}{p}\left(\frac{\mu_X + \mathcal{F}^f(X)}{k_B T}\right) = \sum_i g_i \exp\left(\frac{E_i^{bt} + n_i\mu_{V\mathrm{Fe}} + m_i\mu_X}{k_B T}\right). \tag{11}$$

In this equation, $\mathcal{F}^f(X)$ is an input parameter, which leaves two unknowns: μ_X and $\mu_{V\mathrm{Fe}} = \mu_V - \mu_{\mathrm{Fe}}$. The second equation needed to close the system is Eq. (6) applied for vacancies, and assuming that the total steady-state vacancy concentration is fixed by irradiation conditions and microstructure. Using these two equations [(6) and (11)], we are then able to study the impact of a vacancy supersaturation on the solute concentration in the solid solution, i.e., the solubility limit.

III. PARAMETRIZATION

Using Eq. (11), the equilibrium solute chemical potential can be computed if one knows q/p,$\mathcal{F}^f(X)$, $\mu^{\mathrm{eq}}_{V\mathrm{Fe}}$, and for each excited state i considered: E_i^{bt} and g_i. The ratio q/p is known from the composition of the ordered compound. The other parameters have already been described in depth in Ref. [32]. E_i^{bt} is computed for each excited state using a lattice Hamiltonian that was fitted to density-functional theory (DFT) calculation of small vacancy-solute cluster binding energies. Then an analytical method to explore configurational space allows one to find the energetically most favored configurations. From this method combined with cluster symmetry analysis, the degeneracy of each excited state, g_i, is also obtained. Not too many excited states should be included in the calculation, because of LTE convergence issues (as discussed in Ref. [32]). $\mu^{\mathrm{eq}}_{V\mathrm{Fe}}$ and $\mathcal{F}^f(X)$ are computed with a semi-analytical procedure, combining DFT calculations with experimental data, in which $\mathcal{F}^f(X)$ is assumed linear with respect to temperature:

$$\mathcal{F}^f(X) = E^f(X) - TS^f(X). \tag{12}$$

The energy contribution ($T = 0$ K) is obtained from DFT calculations (FeO system) or fitted to experimental data (FeC and FeN systems), and the entropy contribution is fitted to one high temperature experimental solubility limit, as described in Ref. [32]. The equilibrium chemical potential for replacing one Fe atom by a vacancy $\mu^{\mathrm{eq}}_{V\mathrm{Fe}}$ is assumed to be a function of temperature and magnetization, see Ref. [33], for details,

$$\mu^{\mathrm{eq}}_{V\mathrm{Fe}} = -[\mathcal{F}^f(V)_{|P} + (\mathcal{F}^f(V)_{|F} - \mathcal{F}^f(V)_{|P})M^2], \tag{13}$$

with $\mathcal{F}^f(V)_{|P}$ and $\mathcal{F}^f(V)_{|F}$ being linear functions of temperature. P and F subscripts stand for paramagnetic and ferromagnetic, respectively. M is the magnetization, a function of the temperature and deduced from a mean-field model [41]: $M = \tanh(-MT_C/T)$, and T_C is the Curie temperature ($T_C = 1043$ K in Fe).

Table I summarizes the parameters needed to perform the calculations in this paper. Let us mention that at low temperature ($T < 843$ K), the iron oxide appearing on the phase diagram is magnetite $\mathrm{Fe_3O_4}$. The energy difference in oxygen formation energy from these two possible oxides ($\mathrm{Fe_3O_4}$ and $\mathrm{Fe_{0.947}O}$) has been deduced from thermodynamic assessments of this phase diagram [42] (in eV):

$$\begin{aligned}\mathcal{F}^f(\mathrm{O})_{|\mathrm{Fe}/\mathrm{Fe_3O_4}} = \mathcal{F}^f(\mathrm{O})_{|\mathrm{Fe}/\mathrm{Fe_{0.947}O}} &+ 1.769\times10^{-8}T^2\\ &- 2.829\times10^{-4}T + 0.22813.\end{aligned} \tag{14}$$

TABLE I. Summary of the parameters used in this study.

	C	N	O
$E^f(X)$ (eV) [32]	0.57	0.32	1.28
Experimental $[X]_{\mid\mathrm{sol}}$ at $T_{\mid\mathrm{fit}}$ [appm]	933 [43]	4000 [44]	13 [45]
$T_{\mid\mathrm{fit}}$ [K]	1000	865	1154
Phase $\mathrm{Fe}_p X_q$	$\mathrm{Fe_3C}$	$\mathrm{Fe_4N}$	$\mathrm{Fe_{0.947}O}$
$\mu_X^{\mathrm{eq}}(T_{\mid\mathrm{fit}})$ [eV]	−0.696645	−0.495085	−1.39554
$S^f(X)$ [k_B]	−1.47	−2.36	−0.68
Computed $[X]_{\mid\mathrm{sol}}$ at $T = 300$ K (appm)	2×10^{-4}	1	2×10^{-18}
Maximum cluster size included in the LTE	V_3C_7	V_3N_7	V_3O_5
Pure Fe: $E^f(X)_{\mid P}$ (eV) [32]		2.13	
Pure Fe: $E^f(X)_{\mid F}$ (eV) [46]		1.98	
Pure Fe: $S^f(X)_{\mid P}$ [k_B] [47,48]		5	
Pure Fe: $S^f(X)_{\mid F}$ [k_B] [47,48]		4	

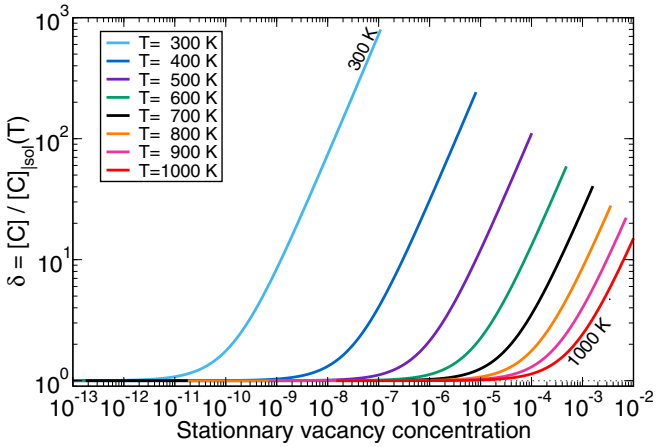

FIG. 1. C solubility limit increase factor as a function of the total steady-state vacancy concentration in the solid solution (concentration per atomic site). The curves from left to right correspond to increasing temperature (300 to 1000 K).

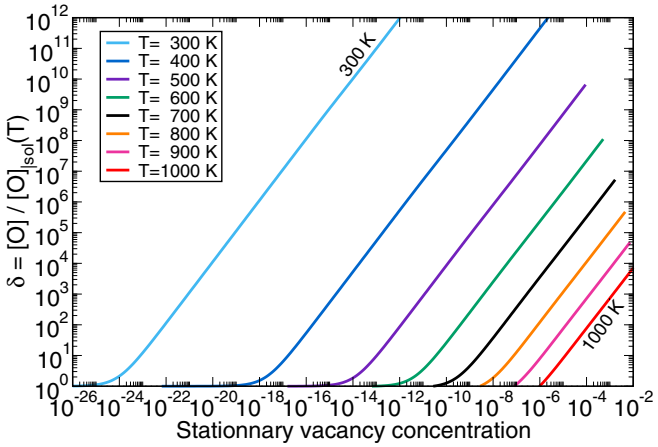

FIG. 3. O solubility limit increase factor as a function of the total steady-state vacancy concentration in the system (concentration per atomic site). The curves from left to right correspond to increasing temperature (300 to 1000 K).

IV. STEADY-STATE SOLUBILITY LIMIT INCREASE UNDER IRRADIATION

A. Vacancy induced dissolution mechanism

With the parameters from Table I, Eq. (11) can now be solved (unknown is μ_X) as a function of the total vacancy concentration in the solid solution, for three different systems: Fe-C (Fig. 1), Fe-N (Fig. 2), and Fe-O (Fig. 3). As a general piece of information, the binding energy between an interstitial solute and a vacancy decreases from O to N to C (1.43, 0.73, and 0.41 eV, respectively), while for a given temperature the solubility limit decreases from N to C to O (∼1000, ∼100, and ∼0.1 appm at $T = 800$ K, respectively). Detailed information on these systems can be found in Ref. [32].

If $\mu_{V\mathrm{Fe}} = \mu^{\mathrm{eq}}_{V\mathrm{Fe}}$ [Eq. (13)], then the equilibrium solubility limit is obtained ($[X]^{\mathrm{eq}}_{|\mathrm{sol}}$). If instead the total vacancy concentration is imposed in the system, and Eq. (6) with $\alpha = V$ is solved to obtain $\mu_{V\mathrm{Fe}}$, then the constrained equilibrium solubility limit is obtained ($[X]^{\mathrm{cons}}_{|\mathrm{sol}}$). "Constrained equilibrium" refers to the fact that vacancies are driven out of their equilibrium concentration by some external process (irradiation, ball milling) but that their nominal concentration does not vary with time (steady state), which allows to define a "constrained" thermodynamic equilibrium between the solid solution and solute precipitates, and thus to define steady-state solubility limit for this constrained equilibrium. Let us define $\delta = \delta(T,[V])$, the solute solubility limit increase factor δ at temperature T due to the nominal vacancy concentration $[V]$:

$$\delta = \delta(T,[V]) = \frac{[X]^{\mathrm{cons}}_{|\mathrm{sol}}}{[X]^{\mathrm{eq}}_{|\mathrm{sol}}}. \tag{15}$$

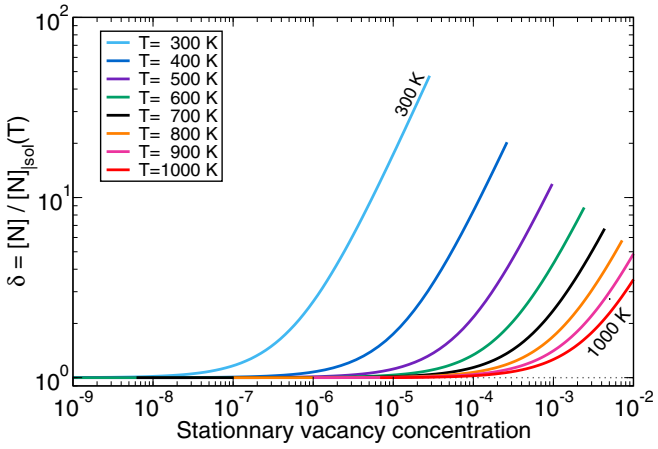

FIG. 2. N solubility limit increase factor as a function of the total steady-state vacancy concentration in the system (concentration per atomic site). The curves from left to right correspond to increasing temperature (300 to 1000 K).

Considering an equilibrium between two phases (solid solution and precipitate), the lever rule gives the volume fraction of the precipitated phase as

$$\frac{v_P}{v_{\mathrm{tot}}} = \frac{\rho_{\mathrm{nom}} - \rho_{SS}}{\rho_P - \rho_{SS}}, \tag{16}$$

where v_P and v_{tot} are the precipitate volume and total system volume, respectively. ρ_{nom} is the nominal solute density (average number of solute per unit volume in the whole system), ρ_{SS} is the equilibrium solute solubility limit (per unit volume of solid solution) and ρ_P is the solute density in the precipitates. Out-of-equilibrium, the precipitate volume becomes [using Eq. (15)]

$$\frac{v^{\mathrm{cons}}_P}{v_{\mathrm{tot}}} = \frac{\rho_{\mathrm{nom}} - \delta \times \rho_{SS}}{\rho_P - \delta \times \rho_{SS}}. \tag{17}$$

It is then possible to express the volume fraction of precipitates that are dissolved due to the stabilization of solutes in the solid solution by association with vacancies

$$\frac{v_P - v^{\mathrm{cons}}_P}{v_P} = \frac{(\delta - 1)\left(\frac{\rho_P}{\rho_{\mathrm{nom}}} - 1\right)}{\left(\delta - \frac{\rho_P}{\rho_{SS}}\right)\left(\frac{\rho_{SS}}{\rho_{\mathrm{nom}}} - 1\right)}, \tag{18}$$

which is always positive. The key quantity in Eq. (18) is δ, which has been computed for all three systems (FeC, FeN, and FeO) as a function of temperature and steady-state vacancy concentration (Figs. 1–3).

All curves show the same trend, whatever the temperature. At low $[V]$, $\delta = 1$, which means that the solubility limit is the same as under equilibrium conditions. There are simply not enough vacancies in the system to form a significant amount of vacancy-solute clusters. At some point, the number of vacancies in the solid solution becomes high enough so that the average solute belonging to the solid solution is more stable than in the equilibrium case. From a LTE perspective [Eq. (5)], the contribution of the excited states to the grand-potential increases, which means that for a given solute concentration, the grand-potential actually decreases. Because two phases in equilibrium must have equal grand-potential, there is a thermodynamic driving force (i.e., a possibility to lower the total energy of the system) by dissolving part of the solute precipitates in the solid solution. Note that the solubility limit increase can be several orders of magnitude, especially for the FeO system.

For each system, the solubility limit increase δ shows a linear trend after some threshold vacancy concentration. The slope is close to 1 at room temperature (0.990, 0.944, and 0.993 for X = C, N and O, respectively), and decreases as temperature increases (0.814, 0.626, and 0.980 at T = 1000 K for X = C, N, and O, respectively). This systematic linear behavior can be qualitatively understood from the LTE formalism, specifically from Eq. (6). Equation (6) tells us that for a given solute chemical potential μ_X, the total vacancy and solute concentration can be expressed as a power series expansion of $\exp(\mu_{V\mathrm{Fe}}/k_BT)$:

$$[V] = \sum_{n\geqslant 1} n(\sigma_V + \sigma_n) \exp\left(\frac{n\mu_{V\mathrm{Fe}}}{k_BT}\right), \tag{19}$$

$$[X] = \sigma_X + \sum_{n\geqslant 1} \tilde{\sigma}_n \exp\left(\frac{n\mu_{V\mathrm{Fe}}}{k_BT}\right). \tag{20}$$

Here, σ_n coefficients represent the contribution of vacancy-solute clusters containing n vacancies, and depend on T and μ_X only. $\tilde{\sigma}_n$ coefficients differ from σ_n coefficients by the weight attributed to each cluster contribution, which depends on the number of vacancies in a cluster for σ_n, and on the number of solutes in a cluster for $\tilde{\sigma}_n$. σ_V (respectively, σ_X) relates to pure vacancy (respectively, solute) clusters in the solid solution. Now we have to make a couple of simplifying assumptions, the main one being that there exists a type of cluster which dominates both the nominal vacancy and solute concentration, labeled m, and containing m_V vacancies and m_X solutes. Also, we assume that vacancy-solute clusters do not affect much the equilibrium solubility limit at room temperature (mostly true), but that under high vacancy supersaturation, these clusters represent the main contribution to the solute nominal concentrations. Equation (19) becomes

$$[V] \simeq m_V\sigma_m \exp\left(\frac{m_V\mu_{V\mathrm{Fe}}}{k_BT}\right). \tag{21}$$

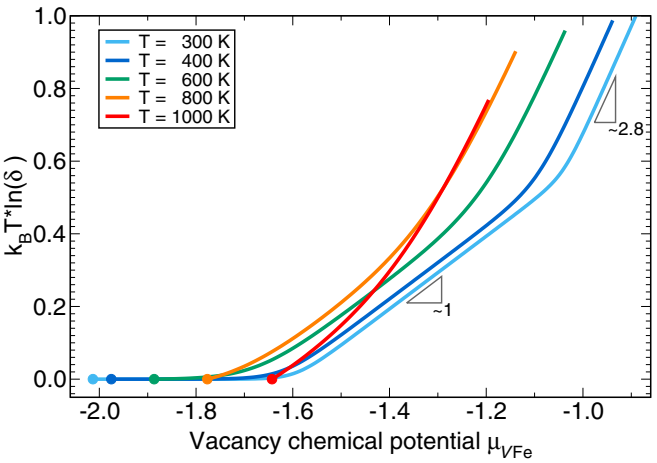

FIG. 4. The solubility limit increase in the FeO system is represented as a function of the vacancy chemical potential $\mu_{V\mathrm{Fe}}$ for various temperatures. The symbols show the equilibrium vacancy chemical potential at each temperature. With our definitions, an increase in the vacancy chemical potential leads to an increase in the total vacancy concentration in the system.

Equation (21) is inserted in Eq. (20),

$$\begin{aligned}\delta = \frac{[X]^{\mathrm{cons}}_{|\mathrm{sol}}}{[X]^{\mathrm{eq}}_{|\mathrm{sol}}} &\simeq 1 + \frac{\tilde{\sigma}_m}{\sigma_X}\exp\left(\frac{m_V\mu_{V\mathrm{Fe}}}{k_BT}\right)\\ &\simeq 1 + \frac{m_X\sigma_m[V]}{m_V\sigma_m\sigma_X}\\ &\simeq \frac{m_X[V]}{m_V\sigma_X},\end{aligned} \tag{22}$$

because when a single cluster m dominates the cluster population, the following equality holds: $\tilde{\sigma}_m = m_X\sigma_m$. This equation clearly shows that in order to have vacancy-induced solubility limit increase, $[V]$ needs to be at least of the order of magnitude of σ_X (solute solubility limit at equilibrium), else the last equality is not valid anymore. Taking the logarithm of Eq. (22), one ends up with the expected linear relation

$$\ln(\delta) = \ln\left(\frac{m_X}{m_V\sigma_X}\right) + \ln([V]). \tag{23}$$

It seems the above assumptions are correct because for all tree systems and each temperature, a linear behavior is observed with a slope close to unity. However, the slope of this law is not exactly one, and decreases with temperature, which is probably due to the fact that at least two clusters may contribute to solute and vacancy concentrations. Additional insight is achieved when $[V]$ in Eq. (23) is replaced by its value in Eq. (21):

$$k_BT\ln(\delta) = k_BT\ln\left(\frac{m_X\sigma_m}{\sigma_X}\right) + m_V\mu_{V\mathrm{Fe}}. \tag{24}$$

Figure 4 represents $k_BT\ln(\delta)$ as function of the vacancy chemical potential $\mu_{V\mathrm{Fe}}$ in the FeO system. If, for a given vacancy concentration range, there is indeed one type of vacancy-solute cluster that dominates the constrained solute solubility limit, it can be found from a linear regression of this plot. Such linear regions are observed and well defined

at low temperature, with successive slopes 0, ∼1, and ∼2.7. Let us discuss for instance the room temperature curve: in the first linear region (slope = 0), vacancies do not affect solute solubility limits. In the second linear region (slope ∼1), vacancy-solute clusters containing one vacancy dominate and explain the solute solubility limit increase. In the third linear region (slope ∼2.7), it seems that a mix of vacancy-solute clusters containing between 2 and 3 vacancies would explain the solute solubility limit increase. The same trend is observed when temperature increases, but the first region narrows, while the transition between region 2 and 3 becomes smoother. Above $T = 800$ K, it seems that the third linear region exists, but not the other ones. This trend is somehow expected, because as temperature increases, the relative stability of each cluster get closer to each other, and it is thus more difficult for one type of cluster to dominate among all others.

Note that previous models of constrained thermodynamics for out-of-equilibrium steady-state systems conclude that large amounts of point defects are required to shift phase diagram boundaries [1,4,5]. Figures 1, 2, and 3 show that it is not the case, because the solute concentration differs by orders of magnitude between the solid solution and the precipitate phase. Hence, a given vacancy concentration changes the average solute energy differently for these two phases, which stabilizes one phase over the other compared with the equilibrium system. The attractive binding energy significantly stabilizes solutes and vacancies in the solid solution, which is the key ingredient to solute solubility limit increase upon V supersaturation. Moreover, the effect on the free energy of the solid solution is not proportional to the vacancy concentration, because clusters larger than vacancy-solute pairs are partly responsible for the stabilization, as evidenced in Fig. 4. Finally, the interaction between vacancies and solutes will most of the time decrease the average diffusivity of vacancies, hence the total concentrations of point defects under irradiation will increase in the alloy compared with the pure material.

Let us summarize and discuss the main result from this section. Under irradiation (or any other vacancy-producing process), we have shown that interstitial solutes (C, N, and O) are stabilized in the solid solution because they form an increased number (compared to equilibrium) of vacancy-solute clusters. This way, solute solubility limits increase under irradiation, and this increase (δ) has been computed as a function of temperature and vacancy supersaturation using LTE. If the system is closed with respect to these solutes (canonical ensemble) then δ allows to predict precipitate dissolution under irradiation [Eq. (18)]. This mechanism of vacancy-induced precipitate dissolution (VID) is an alternative to the well-known dissolution by ballistic effects [7,49,50], and both are compared in the next section. The mechanism presented in this paper is fully based on the mutual stabilization of vacancies and solutes. This requires that solutes and vacancies are able to diffuse to find each other, which requires a not too low temperature. If the temperature is too high, then association between vacancies and solutes does not stabilize the system sufficiently. Hence the proposed mechanism of precipitate dissolution under irradiation is expected to be most efficient at intermediate temperatures, which might help in understanding experiments (e.g., [12,13,15]). Moreover, the LTE calculations are based on the local equilibrium hypothesis, which should be valid at not too high irradiation flux. This hypothesis simply states that it is always possible to define a local volume in the system in which Boltzmann statistics between various possible configurations is obeyed.

B. Comparison between vacancy induced dissolution and ballistic mixing for an interstitial solid solution

In this section, we use simple models to get a quantitative comparison of two solute solubility limit increase (or precipitate dissolution) mechanisms under irradiation: vacancy induced dissolution (VID) and ballistic mixing (BAL). Each of these creates a specific solute solubility limit increase (δ_{VID} and δ_{BAL}, respectively) as a function of various parameters that we introduce below. These two mechanisms are treated as independent and are both operating under irradiation, creating a total solute solubility limit increase $\delta = \delta_{\mathrm{VID}} + \delta_{\mathrm{BAL}}$. As previously, self-interstitial atoms are not treated explicitly and their interaction with solutes is neglected. Their effect only appears implicitly in the recombination term which participates in establishing the total vacancy concentration in the system for given temperature/flux conditions.

Following Martin [50], the solubility limit under irradiation at temperature T is equal to the equilibrium solubility limit at some (higher) effective temperature T_{eff} defined as

$$T_{\mathrm{eff}} = T\left(1 + \frac{D_{\mathrm{bal}}}{\bar{D}_X}\right), \tag{25}$$

where $\bar{D}_X$ is the average solute thermal diffusion coefficient at temperature T and D_{bal} is the ballistic diffusion coefficient, which can be approximated as [50]

$$D_{\mathrm{bal}} = \phi n_{\mathrm{rep}} d_{\mathrm{rec}}^2. \tag{26}$$

Here, ϕ is the irradiation flux (dpa/s), n_{rep} is the number of successive atomic replacement due to a single collision ($n_{\mathrm{rep}} \simeq 10$ for electron irradiation [51]), and d_{rec} is the recoil distance, which we take equal to the first nearest-neighbor distance of the body-centered cubic structure ($d_{\mathrm{rec}} = a\sqrt{3}/2$, a being the lattice parameter). Thermal diffusion of solute X is either due to the diffusion of isolated solutes (for interstitial solutes only) or to the diffusion of vacancy-solute clusters. To simplify the model, it is assumed as in Eq. (22) that one particular vacancy-solute cluster (cluster m containing m_V vacancies and m_X solutes) provides the major contribution to the whole population of vacancy-solute clusters. The average solute thermal diffusion coefficient reads

$$\bar{D}_X = \frac{[X_0]D_X + m_X[m]D_m}{[X_0] + m_X[m]}, \tag{27}$$

where D_X and D_m are the diffusion coefficients of isolated solute and cluster m, respectively, and $[X_0]$ and $[m]$ are the corresponding concentrations. Assuming local equilibrium,

$$[m] = [X_0]^{m_X}[V_0]^{m_V} Z_m, \tag{28}$$

where $[V_0]$ is the concentration of isolated vacancies, and Z_m is the exponential of the binding free energy of cluster m. Let $\mathcal{F}^f(X)$ be the free formation energy of solute X in the solid solution (from a given precipitated phase of this solute or solute reservoir). Note that in principle $\mathcal{F}^f(X)$ can depend on the vacancy concentration in the system. Then the isolated solute

concentration is expressed as $[X_0] = \exp(-\mathcal{F}^f(X)/k_BT)$. The vacancy monomer concentration $[V_0]$ is deduced from the total vacancy concentration:

$$[V] = [V_0] + m_V[m]. \tag{29}$$

The solute supersaturation due to ballistic mixing is then

$$\delta_{\mathrm{BAL}} = \frac{[X]^{\mathrm{cons}}_{|\mathrm{sol}}}{[X]^{\mathrm{eq}}_{|\mathrm{sol}}} = \exp\left(-\frac{\mathcal{F}^f(X)}{k_BT_{\mathrm{eff}}} + \frac{\mathcal{F}^f(X)}{k_BT}\right), \tag{30}$$

which can be rewritten in a more convenient form

$$\ln(\delta_{\mathrm{BAL}}) = \frac{\mathcal{F}^f(X)}{k_BT}\left(\frac{1}{1+\bar{D}_X/D_{\mathrm{bal}}}\right). \tag{31}$$

For the VID mechanism, we simply use Eq. (23) in which σ_X is being replaced by $[X]^{\mathrm{eq}}_{|\mathrm{sol}} = \exp(-\mathcal{F}^f(X)/k_BT)$,

$$\ln(\delta_{\mathrm{VID}}) = \ln\left(\frac{m_X}{m_V}\right) + \frac{\mathcal{F}^f(X)}{k_BT} + \ln([V]), \tag{32}$$

where $[V]$ is the total vacancy concentration in the system. Following rate theory models (e.g., Refs. [5,8,51]), the total steady-state vacancy concentration under irradiation can be estimated as

$$[V] = -\frac{k^2\Omega}{8\pi r_c} + \sqrt{\left(\frac{k^2\Omega}{8\pi r_c}\right)^2 + \frac{\phi\Omega}{4\pi r_c\bar{D}_V}}, \tag{33}$$

where $\Omega = a^3/2$ is the atomic volume, r_c is the capture radius below which vacancy and self-interstitial spontaneously recombine (estimated as $r_c = \sqrt{3}a$ [51]), k^2 is the sink strength which depends on microstructure and irradiation conditions (assumed unbiased for simplicity, typical values range between 10^{12} and 10^{19} m^{-2} [51]), and $\bar{D}_V$ is the average vacancy diffusion coefficient, defined similarly as Eq. (27):

$$\bar{D}_V = \frac{[V_0]D_V + m_V[m]D_m}{[V_0] + m_V[m]}. \tag{34}$$

We now apply this model to the case of oxygen in α-Fe to identify the temperature/irradiation flux regions where ballistic mixing and/or vacancy induced dissolution is the dominant mechanism. For the VID mechanism, the most probable vacancy-oxygen cluster is VO_2. In the FeO system, it has been computed that the oxygen chemical potential does not vary much with the vacancy supersaturation (the relative variation is lower than 10^{-5} for $T \leqslant 700$ K), such that we assume $[O_0] = [O]^{\mathrm{eq}}_{|\mathrm{sol}} = \exp(-\mathcal{F}^f(O)/k_BT)$ for simplicity, where $\mathcal{F}^f(O)$ is the equilibrium oxygen formation energy. Note that O diffuses according to an interstitial mechanism in αFe, which, contrary to substitutional solutes, does not require a vacancy. This is a major difference compared to previous studies of ballistic mixing (e.g., Refs. [50,51]). Table II lists the values of all the parameters needed in Eqs. (26)–(34), and shows that VO_2 clusters diffuse much slower than isolated O atoms; therefore, increasing the concentration of point defects would actually reduce the average diffusivity of interstitial solutes, whereas it increases the average diffusivity of substitutional solutes. Yet, most of the O atoms are isolated unless the vacancy concentration is very large, such that the average O diffusivity does not vary much under irradiation. Looking at Eq. (34) and the values in Table II, O atoms will slow down vacancies, which leads to an increase in the total V concentration under irradiation, and thus increases the stabilization of O atoms in the solid solution.

TABLE II. List of the parameters used for the comparison between VID and BAL mechanisms. Irradiation parameters have been set to standard values for electron irradiation. All the k_BT terms in this table must be expressed in eV.

Parameter	Units	Value	Reference
$\mathcal{F}^f(X)$	eV	1.51–$3.47k_BT$	[32,33]
m_V	–	1	This work
m_X	–	2	This work
Z_m	–	$3\exp\left(-\frac{3.04}{k_BT}\right)$	[32]
a	m	2.88×10^{-10}	[32]
D_m	m^2/s	$10^{-6}\exp\left(-\frac{2.06}{k_BT}\right)$	[52]
D_V	m^2/s	$6.7\times10^{-6}\exp\left(-\frac{0.67}{k_BT}\right)$	[53,24]
D_X	m^2/s	$10^{-6}\exp\left(-\frac{0.54}{k_BT}\right)$	[54,24]
n_{rep}	–	10	[51]
k^2	m^{-2}	10^{15}	[51]

Figure 5 shows the computed total vacancy concentration in the system [Eq. (33)] as a function of temperature and irradiation flux. The black lines define four regions (from left to right): in the first region, the BAL mechanism dominates; in the narrow second region, BAL and VID mechanisms are about the same order of magnitude; in the third region, VID mechanism dominates; in the fourth region, none of these mechanisms is efficient. The VID mechanism requires a lot of vacancies, so it is expected to be most efficient at low/intermediate temperatures, which is observed. The BAL mechanism is

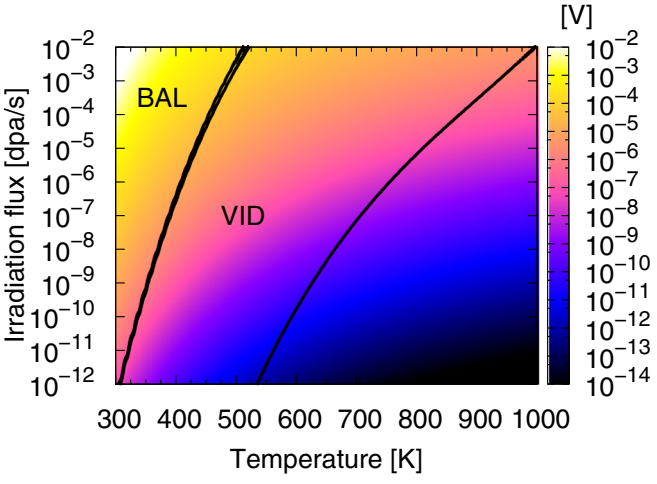

FIG. 5. Total vacancy concentration $[V]$ in the system as a function of temperature and irradiation flux obtained with the parameters from Table II. In the "VID" (respectively, "BAL") region, vacancy induced dissolution (respectively, ballistic mixing) is the main mechanism responsible for solute solubility limit increase. See Fig. 6 for more details.

most efficient at low temperature because thermal diffusion is slower, so it is harder for atoms ejected from a given equilibrium state to diffuse back to this state. Figure 5 also enables to relate, at least roughly, the abscissa of Figs. 1–3, to typical temperature/irradiation flux conditions.

Figure 6 shows the total solute supersaturation δ as a function of temperature and irradiation flux. The black lines define the same regions as in Fig. 5 (see previous paragraph). The first plot [Fig. 6(a)] uses the parameters from Table II, and the corresponding total vacancy concentration is the one plotted in Fig. 5. At low temperature/high irradiation flux, both mechanisms contribute significantly to solute solubility limit increase, but the BAL mechanism is much more efficient. Moreover, the VID contribution is probably overestimated in this region because diffusion is slow, so it takes a significant amount of time before local equilibrium is reached. At intermediate temperatures and irradiation fluxes, the VID mechanism dominates. The region in between where the solute supersaturation coming from each mechanism is about the same order of magnitude is narrow, which supports our assumption that both mechanisms are independent. When irradiation flux becomes too low and/or temperature too high, then none of these mechanisms produces any significant solute supersaturation.

It is shown in Ref. [51] that as irradiation goes on, more and more point defect clusters form and grow, and this leads to an increase in the overall sink strength. Higher sink strength leads to lower point defect concentration in the system, and thus to a reduced efficiency of the VID mechanism. To confirm the effect of this microstructure evolution, Fig. 6(b) shows the exact same calculation as previously except that the sink strength has been increased from $k^2 = 10^{15}$ to 10^{19} m^{-2}. The BAL region is not much affected by this change [compared to Fig. 6(a)], whereas the VID region is not as large as in the previous case, and δ_{VID} is lower for a given temperature and irradiation flux.

All this discussion has been made for interstitial solutes. The main difference with substitutional solutes is that the latter are immobile as isolated species (they need a point defect to diffuse) while the former are mobile. To get a rough idea of how the BAL/VID boundary evolves for substitutional solutes, we used the same set of parameters as in Fig. 6(a), except that the isolated solute diffusion coefficient D_X was set to zero. Figure 6(c) shows that the BAL region expands to much higher temperatures and lower irradiation fluxes, which is expected: setting D_X to zero reduces the average solute diffusivity $\bar{D}_X$, which explicitly appears in the calculation of δ_{BAL} [Eq. (31)]. Physically, it is harder for solute ejected by irradiation particles to diffuse back to their equilibrium state. On the contrary, this change should not have much effect on the δ_{VID}, except that it might be harder to reach the required local equilibrium (but this feature is not taken into account in this simple model). Let us point out that Fig. 6(c) is not quantitatively relevant for substitutional solutes, because these usually have much higher solubility limits and much lower vacancy-solute binding than oxygen. Similar graphs for substitutional solutes will be the focus of a future paper.

Figure 6 provides a map to estimate the temperature/irradiation flux conditions in which BAL or VID mechanisms would be relevant. As expected, BAL dominates at low temperature/high flux while VID dominates at intermediate temperature and irradiation flux.

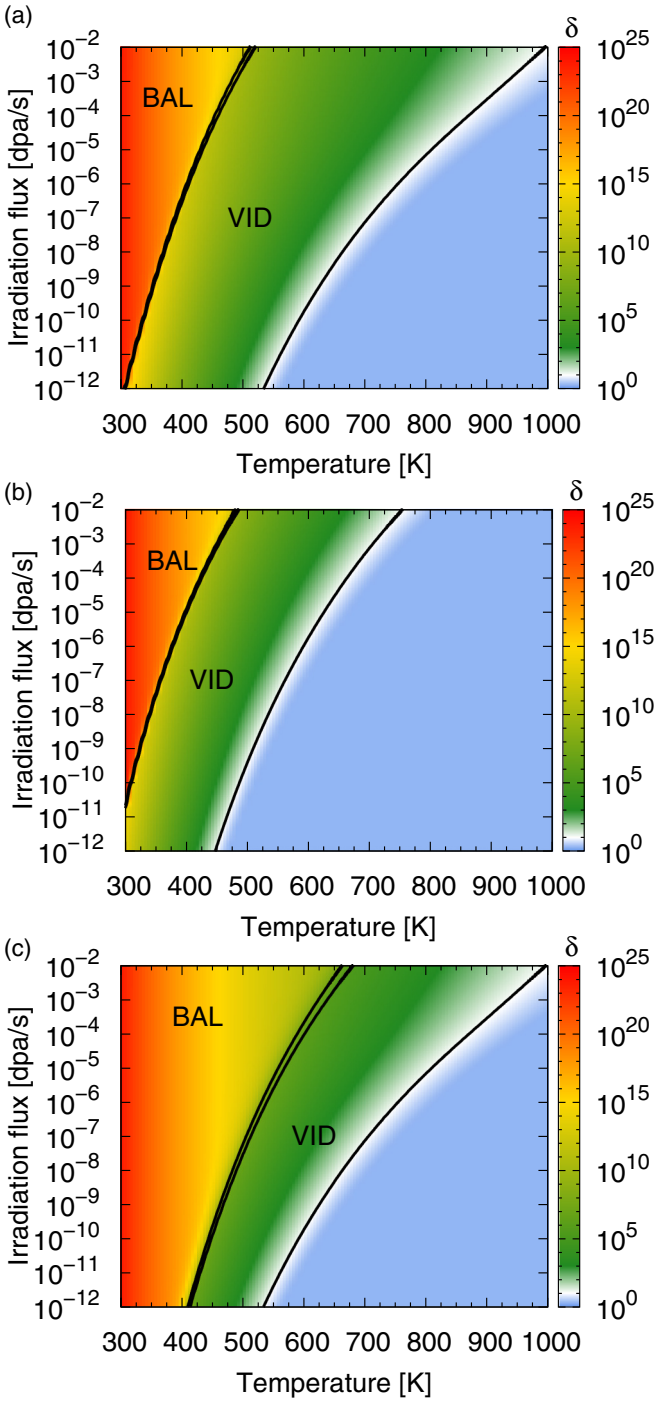

FIG. 6. Total solubility limit increase under irradiation $\delta = \delta_{\mathrm{VID}} + \delta_{\mathrm{BAL}}$ as a function of temperature and irradiation flux. (a) has been computed with the parameters in Table II. In (b), the sink strength was increased from $k^2 = 10^{15}$ to 10^{19} m^{-2}. In (c), the sink strength is set back to its original value but isolated solutes are considered immobile ($D_X = 0$). For each plot, there are four main regions: BAL region (defined as $\delta_{\mathrm{BAL}} \geqslant 10\delta_{\mathrm{VID}}$); a narrow transition region where both mechanism (VID and BAL) are of similar magnitudes; VID region (defined as $\delta_{\mathrm{VID}} \geqslant 10\delta_{\mathrm{BAL}}$); the blue region in the bottom right-hand side corner where none of these mechanisms affects the system ($\delta \simeq 1$).

V. POTENTIAL APPLICATIONS

A. Assessment of ODS particles stability under irradiation

Oxide-dispersed strengthen (ODS) steels are candidates for future nuclear reactor applications because of their good mechanical properties at high temperature and their resistance to swelling and creep deformation [11]. Schematically, they consist of a ferritic-martensitic FeCr matrix in which a homogeneous distribution of small oxide particles is inserted by ball milling. These oxides are found to have the nearly stoichiometric pyrochlore structure $Y_2Ti_2O_7$, at least for the ones larger than 5 nm [55]. For a sustainable use of these materials in nuclear environment, it is crucial to assess the stability of the ODS microstructure under irradiation. From some experimental observations, the nano-oxide particles seem to be stable under irradiation [15,56] but other studies observe particles dissolution under irradiation [12–15,18–20,57,58], see Ref. [16] for a review. These studies stress that ballistic mixing models do not quantitatively account for the observed dissolution phenomenon. Also, it is much more efficient in electron irradiation samples compared with ion irradiation samples, which underlines the role of isolated point defects [12].

Unfortunately, it is not yet possible to assess whether the VID mechanism fully accounts for experimental observations using Eq. (18) and/or Fig. 6, because a number of issues remains. (1) The steady-state of the system is often not reached in experiments. (2) The measured oxygen concentration in the solid solution is orders of magnitude above the experimental solubility limits, even before irradiation [59,60]. (3) A correct assessment of precipitate dissolution should involve five species (Fe-Cr-Y-Ti-O), either with canonical (fixed concentration) or grand-canonical (fixed chemical potential) conditions for each of them. Such a complete simulation of ODS steels is beyond the scope of this paper, and more data would be required. (4) The interface energy of the precipitates, as well as their possible off-stoichiometry, will probably have an important influence on precipitate dissolution [32].

From a qualitative point of view, and treating the ODS alloy as an FeO alloy, Fig. 6(a) shows that the precipitate dissolution stems from the VID mechanism in the following regions where experiments where performed: $3 - 6 \times 10^{-3}$ dpa/s and 573–823 K [12]; 1.4×10^{-3} dpa/s 773–973 K [13]; 1.4×10^{-2} dpa/s 573–873K [18]; and 0.5×10^{-5} dpa/s 673K. To simplify the discussion, we did not distinguish between various types of irradiation particles, but the qualitative observation that VID is the dominant dissolution mechanism is still valid if irradiation rates are decreased by 1–2 orders of magnitude to account for point-defect production efficiency. The fact that precipitate dissolution occurs for electron irradiated samples demonstrates that cascades are not part of the mechanism [12]. Yet, Monnet *et al.* [12] show that a threshold irradiation energy is needed to observe the dissolution, which they interpret as the energy needed to displace Y atoms. In our simplified model, we consider only FeO precipitates and evaluate the tendency for O to go into the solid solution. In a more realistic ODS particle, the dissociation of O from the oxide raises the question of changes in the stoichiometry, which might at some point limit the dissolution. The dissociation of O atoms only could explain the Y-enriched shell observed around some precipitates after irradiation [58] and the change in oxide stoichiometry

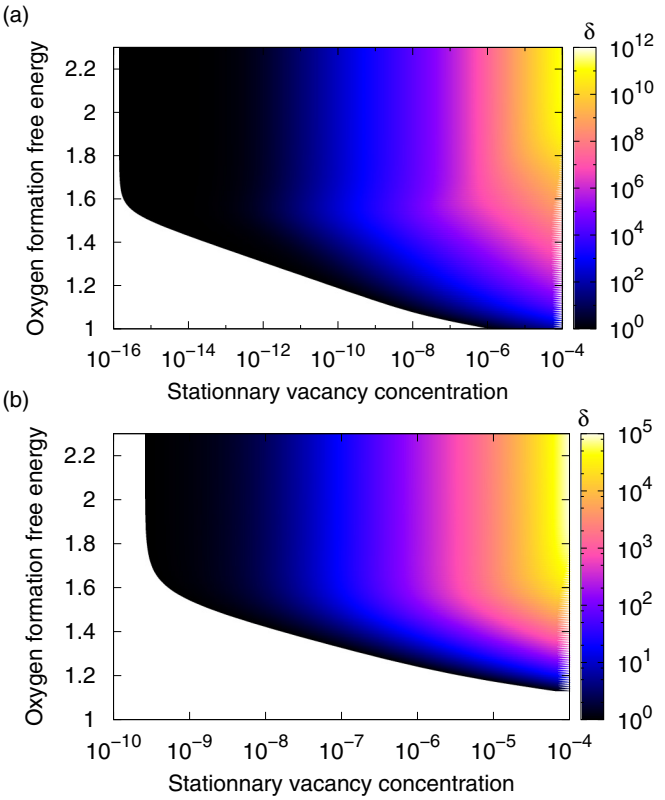

FIG. 7. Oxygen solubility limit increase δ as a function of the steady-state concentration of vacancies (per atomic site) and the oxygen formation free energy $\mathcal{F}^f$(O) (eV). The latter is the energy difference between an oxygen atom belonging to the oxide, and an oxygen atom isolated in the solid solution. The oxide has the stoichiometry Fe_4O_7. Temperature is set to (a) $T = 600$ and (b) 900 K.

[12,58]. Moreover, it has been shown that the dissolution rate depends on the particle chemical composition [14], which is represented as the oxygen formation energy in our model (see Fig. 7 hereafter). The nonlinear effect of temperature on precipitate dissolution is also a commonly observed feature [12–14,18], and some author explain these variations by a balance between ballistic effects and radiation-enhanced diffusion [18]. Let us stress that there is no radiation-enhanced diffusion for oxygen atoms because they diffuse as interstitial species. Looking at Fig. 6, temperature has two contradictory effects on the VID mechanism: as temperature increases, δ_{VID} decreases because the formation of vacancy-solute clusters is less probable; but higher temperatures favor the thermal dissociation of an oxygen atom from the oxide, as well as its diffusion in the solid solution, thus its probability to pair with a vacancy. It is thus expected that precipitate dissolution would be more kinetically effective at higher temperatures, even if the steady-state precipitated volume fraction would be lower.

A first estimation of δ, the oxygen solubility increase can be obtained from our calculations. Compared to the ODS system, we have to make simplifying assumptions. First, we assume that each substitutional atom has the same energy as an Fe atom. The stoichiometry of the oxide is thus chosen as Fe_4O_7 (from $Y_2Ti_2O_7$). As the solubility limit of oxygen in Fe at equilibrium with nano-oxides is unknown, and as the

steady-state vacancy supersaturation is unknown as well, we perform a parametric study over these two parameters, the former being derived from the oxygen formation energy $\mathcal{F}^f(\mathrm{O})$. The results are plotted in Fig. 7 for two temperatures: $T = 600$ and 900 K.

Figure 7(a) shows that at low $\mathcal{F}^f(\mathrm{O})$, the equilibrium vacancy concentration (black, $\delta = 1$) is already very high (a few appm). As $\mathcal{F}^f(\mathrm{O})$ increases, the concentration of O atoms in the solid solution decreases and it is less probable to form vacancy-oxygen clusters. Thus vacancies are less stabilized by oxygen and the equilibrium vacancy concentration decreases, up to a point where oxygen atoms do not affect the equilibrium vacancy concentration at all ($\mathcal{F}^f(\mathrm{O}) \geqslant 1.7$ eV), and all vacancies in the system are isolated vacancies. For a given value $\mathcal{F}^f(\mathrm{O})$, increasing the total vacancy concentration in the system (irradiation) increases δ. At low $\mathcal{F}^f(\mathrm{O})$, high vacancy concentrations are needed to increase δ because there is already a high concentration of vacancy-solute clusters in the solid solution at equilibrium. For higher $\mathcal{F}^f(\mathrm{O})$, it seems that vacancy concentrations as low as 10^{-10} are sufficient to increase the oxygen solubility limits by 2–4 orders of magnitude. Let us emphasize that as $\mathcal{F}^f(\mathrm{O})$ increases, the equilibrium oxygen solubility limit decreases, and δ is the solubility limit increase with respect to this equilibrium O solubility limit.

Figure 7(b) shows the same data at a higher temperature ($T = 900$ K). The trend is similar to the previous plot, but equilibrium oxygen solubility limits are higher than at $T = 600$ K, it is thus more difficult to create a high oxygen supersaturation δ. This is reflected in the color scale, which only goes up to five orders of magnitude (instead of 12 orders of magnitude at $T = 600$ K). The comparison between these two graphs shows that for a given $\mathcal{F}^f(\mathrm{O})$ and vacancy supersaturation, the solubility limit increase is very sensitive to temperature. The solubility limit increase is obviously less important at high temperatures. Nevertheless, one has to keep in mind that the mutual stabilization of vacancies and oxygen atoms is possible only if they are able to diffuse. In this sense, higher temperatures make it easier for the system to reach the steady-state microstructure.

B. Measurement of vacancy concentration in out-of-equilibrium systems

The supersaturation of point defects in out-of-equilibrium systems is a crucial quantity as it directly relates to the driving force for point defect elimination. In the framework of the thermodynamics of irreversible processes, the fluxes of point defect, and the fluxes of solutes (because of flux coupling) are proportional to these driving forces [25]. Thus knowing point defect supersaturation is necessary to be able to predict solute redistribution.

Yet, reliable measurements of point defect supersaturations are scarce. Some attempts have been made using positron annihilation spectroscopy, but the analysis of the results remains difficult [61,62]. In pure metals, it seems that rate theory models give an accurate description [8,63], but their application to alloys is much more complicated.

Results from the previous section show that the free energy curve of the solid solution depends on the interplay between vacancies and solutes. In other words, it means that vacancy

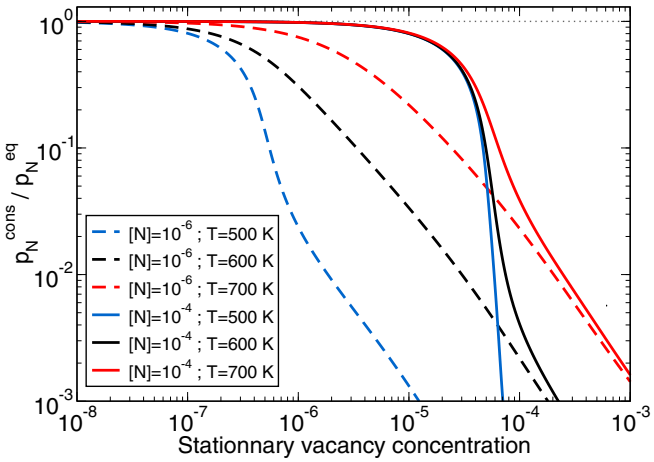

FIG. 8. LTE calculation of the ratio $p_{\mathrm{N}}^{\mathrm{cons}}/p_{\mathrm{N}}^{\mathrm{eq}}$ as a function of the steady-state out-of-equilibrium vacancy concentration (per site) in the system. Dashed curves are for low N concentration in the system ([N] = 1 appm), and solid curves are for higher concentrations ([N] = 100 appm). Colors relate to temperature: $T = 500$ (blue), 600 (black), and 700 K (red).

and solute chemical potentials affect each other, as it appears in Eqs. (6) and (11). The solute chemical potential μ_X is in some conditions measurable because it relates to the solute partial pressure p_X [64],

$$\mu_X = \mu_{\mathrm{REF}} + k_B T \ln(p_X), \tag{35}$$

where μ_{REF} is the solute chemical potential in a given reference state. The LTE calculations provide the link between μ_X and $\mu_{V\mathrm{Fe}}$, so if we can measure μ_X we have an indirect estimation of $\mu_{V\mathrm{Fe}}$. From this observation, we introduce the principle of an experiment dedicated to the measure of out-of-equilibrium point defect concentrations and point defect diffusion driving forces. It is illustrated on the case of vacancy supersaturation measurements in FeN alloys, because among the three solutes studied in this paper, N is the one whose chemical potential is most sensitive to the vacancy supersaturation.

Assume a closed system in equilibrium conditions: a sample of ferrite in solid solution containing some amount of nitrogen (below the solubility limit), at equilibrium with the surrounding vacuum in which the partial pressure of N is measured and equal to $p_{\mathrm{N}}^{\mathrm{eq}}$. Now the external force driving the system out-of-equilibrium (e.g., irradiation) is turned on, and one can follow the nitrogen partial pressure evolution, which equals $p_{\mathrm{N}}^{\mathrm{cons}}$ once steady-state is reached. Using Eq. (35),

$$\frac{p_{\mathrm{N}}^{\mathrm{cons}}}{p_{\mathrm{N}}^{\mathrm{eq}}} = \exp\left(\frac{\mu_{\mathrm{N}}^{\mathrm{cons}} - \mu_{\mathrm{N}}^{\mathrm{eq}}}{k_B T}\right). \tag{36}$$

The system is closed, so the total N concentration is known. The measurement of partial pressures is directly related to the constrained equilibrium N chemical potential. Using Eq. (6) for $\alpha = \mathrm{N}$, one can solve for the vacancy chemical potential in out-of-equilibrium conditions, and from that use Eq. (6) for $\alpha = V$ to compute the steady-state vacancy concentration in the system.

Figure 8 shows a parametric study of the computed evolution of the ratio $p_{\mathrm{N}}^{\mathrm{cons}}/p_{\mathrm{N}}^{\mathrm{eq}}$ as a function of the total

vacancy concentration in the system. This kind of plot shows that the measurement is sensitive to temperature and N nominal concentration, and these dependencies are strongly nonlinear. It can be provided as abacus plots to avoid going through solving LTE equations for each measurement.

VI. CONCLUSION

In this paper, we presented a quantitative and consistent method for computing both vacancy-induced and ballistic precipitate dissolution with a unified formalism, starting from the atomic scale. It is straightforward to extend the same approach to other types of defects (self-interstitials, dislocation loops, dislocations, etc.). If the point defect concentration concentration is about the same order of magnitude as the solute concentration, and if these point defects show an attractive binding with solutes, then the solutes will be stabilized in the solid solution by forming point defect-solute clusters. The out-of-equilibrium dynamic solubility is then higher than the equilibrium solubility limit, hence the partial dissolution of equilibrium precipitates.

Assuming that the system obeys local equilibrium, LTE calculations were used to compute the steady-state solubility limit increase (up to several orders of magnitude) as a function of the vacancy nominal concentration and temperature. Oxygen atoms were shown to be very sensitive to the vacancy supersaturation in the solid solution, mainly due to the highly attractive binding energy between a vacancy and an oxygen atom in Fe (1.43 eV [32]). Therefore we expect the VID mechanism to be very efficient on O-rich precipitates in α-Fe. Larger vacancy concentrations would be needed to produce a partial dissolution of N-rich and C-rich precipitates in α-Fe.

This mechanism is most likely to be effective at intermediate temperatures. (1) Temperature must be high enough so that solutes and point defects can actually diffuse, dissociate from solute precipitates and meet to form clusters in the solid solution. (2) If the temperature is too high, then point defect solute clusters will not form to minimize the overall free energy of the system (comparison between the configurational entropy gain of having isolated solutes and point defects separated and the enthalpy gain of forming point defect solute clusters). The VID mechanism is an alternative to the well-known ballistic mixing effect. The latter has been shown to be the dominant mechanism at low temperatures and high fluxes and it is restricted to irradiation. Also, the VID mechanism is likely to be effective in sustained out-of-equilibrium systems other than irradiated materials, for instance, ball milling or severe plastic deformation. For a given irradiation flux, the VID mechanism has a lower effect on dynamic solubility limits than ballistic mixing, but it operates at higher temperatures. Moreover, note that the attractive interaction between vacancies and solutes will in most cases decrease the average vacancy diffusivity and thus increase the total vacancy concentration in the irradiated solid solution, and this kinetic effect is taken into account in our model.

We also discussed ODS particle stability. Quantitative assessment would require a more complex model, but our calculations show that the VID mechanism is much more effective than ballistic mixing in the high temperature/high irradiation flux region that corresponds to experiments where ODS particles dissolution is observed under irradiation [12–14,16,18]. Finally, we presented a potential application of these calculations: the measurement of out-of-equilibrium vacancy concentrations and diffusion driving forces from solute partial pressures, a quantity which lacks reliable experimental measurements.

Future work should focus on two aspects. (1) The extension of the LTE model and parametrization to ternary systems, to clearly identify the thermodynamic forces for precipitate dissolution in out-of-equilibrium systems when these precipitates are composed of two solutes. (2) Experimental verification of our model is now desired on model systems, for instance Al_2O_3, MgO and/or Y_2O_3 in pure Fe for which it is possible to provide quantitative information, instead of the FeCr matrix used in Ref. [14].

ACKNOWLEDGMENTS

The authors thank Georges Martin for stimulating discussions. This work was supported by the joint program "CPR ODISSEE" funded by AREVA, CEA, CNRS, EDF and Mécachrome under Contract No. 070551. This work has been carried out partially within the framework of the EUROfusion Consortium and has received funding from the Euratom research and training program 2014-2018 under Grant Agreement No. 633053. The views and opinions expressed herein do not necessarily reflect those of the European Commission.

[1] J. P. Holloway and J. F. Stubbins, J. Nucl. Mater. **122**, 591 (1984).
[2] S. Maydet and K. Russell, J. Nucl. Mater. **64**, 101 (1977).
[3] R. Nelson, J. Hudson, and D. Mazey, J. Nucl. Mater. **44**, 318 (1972).
[4] J.-L. Bocquet and G. Martin, J. Nucl. Mater. **83**, 186 (1979).
[5] K. Russell, Prog. Mater. Sci. **28**, 229 (1984).
[6] G. Martin and P. Bellon, Solid State Phys. **50**, 189 (1996).
[7] R. A. Enrique and P. Bellon, Phys. Rev. Lett. **84**, 2885 (2000).
[8] G. Was, *Fundamentals of Radiation Materials Science* (Springer, Berlin, Heidelberg, 2007).
[9] S. Shu, P. Bellon, and R. S. Averback, Phys. Rev. B **91**, 214107 (2015).
[10] S. J. Zinkle and J. T. Busby, Mater. Today **12**, 12 (2009).
[11] J.-L. Boutard, V. Badjeck, L. Barguet, C. Barouh, A. Bhattacharya, Y. Colignon, C. Hatzoglou, M. Loyer-Prost, A. Rouffié, N. Sallez *et al.*, J. Nucl. Mater. **455**, 605 (2014).
[12] I. Monnet, P. Dubuisson, Y. Serruys, M. Ruault, O. Kaïtasov, and B. Jouffrey, J. Nucl. Mater. **335**, 311 (2004).
[13] T. Allen, J. Gan, J. Cole, M. Miller, J. Busby, S. Shutthanandan, and S. Thevuthasan, J. Nucl. Mater. **375**, 26 (2008).
[14] I. Monnet, T. Van den Berghe, and P. Dubuisson, J. Nucl. Mater. **424**, 204 (2012).
[15] M.-L. Lescoat, J. Ribis, Y. Chen, E. Marquis, E. Bordas, P. Trocellier, Y. Serruys, A. Gentils, O. Kaïtasov, Y. de Carlan *et al.*, Acta Mater. **78**, 328 (2014).
[16] M. Swenson and J. Wharry, J. Nucl. Mater. **467**, 97 (2015).

[17] F. Li, H. Abe, T. Ishizaki, Y. Li, T. Nagasaka, T. Muroga, T. Nagase, and H. Yasuda, J. Nucl. Mater. **455**, 724 (2014).

[18] J. He, F. Wan, K. Sridharan, T. R. Allen, A. Certain, V. Shutthanandan, and Y. Wu, J. Nucl. Mater. **455**, 41 (2014).

[19] T. Chen, E. Aydogan, J. G. Gigax, D. Chen, J. Wang, X. Wang, S. Ukai, F. Garner, and L. Shao, J. Nucl. Mater. **467**, 42 (2015).

[20] T. Chen, J. G. Gigax, L. Price, D. Chen, S. Ukai, E. Aydogan, S. Maloy, F. Garner, and L. Shao, Acta Mater. **116**, 29 (2016).

[21] M. Nastar, Philos. Mag. **85**, 3767 (2005).

[22] V. Barbe and M. Nastar, Philos. Mag. **86**, 3503 (2006).

[23] L. Messina, M. Nastar, T. Garnier, C. Domain, and P. Olsson, Phys. Rev. B **90**, 104203 (2014),

[24] T. Schuler and M. Nastar, Phys. Rev. B **93**, 224101 (2016).

[25] M. Nastar and F. Soisson, Comprehen. Nucl. Mater. **1**, 471 (2012).

[26] R. Hu, G. D. Smith, and E. A. Marquis, Prog. Nucl. Energy **57**, 14 (2012).

[27] J. Piochaud, M. Nastar, F. Soisson, L. Thuinet, and A. Legris, Comput. Mater. Sci. **122**, 249 (2016).

[28] A. J. Ardell and P. Bellon, Curr. Opin. Solid State Mater. Sci. **20**, 115 (2016).

[29] A. Barbu and A. Ardell, Scr. Metall. **9**, 1233 (1975).

[30] P. Pareige, B. Radiguet, and A. Barbu, J. Nucl. Mater. **352**, 75 (2006).

[31] R. Cauvin and G. Martin, J. Nucl. Mater. **83**, 67 (1979).

[32] C. Barouh, T. Schuler, C.-C. Fu, and M. Nastar, Phys. Rev. B **90**, 054112 (2014).

[33] T. Schuler, C. Barouh, M. Nastar, and C.-C. Fu, Phys. Rev. Lett. **115**, 015501 (2015).

[34] M. F. Sykes, J. Math. Phys. **14**, 1060 (1973).

[35] F. Ducastelle, *Order and Phase Stability in Alloys, Cohesion and Structure* (North-Holland, Amsterdam, 1991).

[36] A. Kohan, P. Tepesch, G. Ceder, and C. Wolverton, Comput. Mater. Sci. **9**, 389 (1998).

[37] M. Asta, S. M. Foiles, and A. A. Quong, Phys. Rev. B **57**, 11265 (1998).

[38] R. Hyland, M. Asta, S. Foiles, and C. Rohrer, Acta Mater. **46**, 3667 (1998).

[39] Y. Le Bouar, A. Loiseau, and A. Finel, Phys. Rev. B **68**, 224203 (2003).

[40] E. Clouet and M. Nastar, Phys. Rev. B **75**, 132102 (2007).

[41] L. Ruch, D. R. Sain, H. L. Yeh, and L. Girifalco, J. Phys. Chem. Solids **37**, 649 (1976).

[42] B. Sundman, J. Phase Equili. **12**, 127 (1991).

[43] J. Chipman, Metall. Trans. **3**, 55 (1972).

[44] H. A. Wriedt, N. A. Gokcen, and R. H. Nafziger, Bull. Alloy Phase Diagr. **8**, 355 (1987).

[45] J. Swisher and E. Turkdogan, Trans. Metall. Soc. AIME **239**, 426 (1967).

[46] H. Ding, V. I. Razumovskiy, and M. Asta, Acta Mater. **70**, 130 (2014).

[47] H. Wen, P.-W. Ma, and C. Woo, J. Nucl. Mater. **440**, 428 (2013).

[48] H. Wen and C. Woo, J. Nucl. Mater. **455**, 31 (2014).

[49] K. C. Russell, J. Nucl. Mater. **83**, 176 (1979).

[50] G. Martin, Phys. Rev. B **30**, 1424 (1984).

[51] F. Soisson and T. Jourdan, Acta Mater. **103**, 870 (2016).

[52] C. Barouh, T. Schuler, C.-C. Fu, and T. Jourdan, Phys. Rev. B **92**, 104102 (2015),

[53] C.-C. Fu, J. D. Torre, F. Willaime, J.-L. Bocquet, and A. Barbu, Nat. Mater. **4**, 68 (2004).

[54] *Landolt-Börnstein - Volume 26: Diffusion in Solid Metals*, edited by H. Mehrer (Springer-Verlag, Berlin, Heidelberg, 1990).

[55] V. Badjeck, M. Walls, L. Chaffron, J. Malaplate, and K. March, J. Nucl. Mater. **456**, 292 (2015).

[56] P. Pareige, M. Miller, R. Stoller, D. Hoelzer, E. Cadel, and B. Radiguet, J. Nucl. Mater. **360**, 136 (2007).

[57] P. Dubuisson, R. Schill, M.-P. Hugon, I. Grislin, and J.-L. Seran, in *Effects of Radiation on Materials: 18th International Symposium* (ASTM International, West Conshohocken, PA, 1999), p. 882.

[58] J. He, F. Wan, K. Sridharan, T. R. Allen, A. Certain, and Y. Wu, J. Nucl. Mater. **452**, 87 (2014).

[59] S.-Y. Zhong, J. Ribis, N. Lochet, Y. de Carlan, V. Klosek, V. Ji, and M.-H. Mathon, Metall. Mater. Trans. A **46**, 1413 (2014).

[60] L. Barnard, N. Cunningham, G. Odette, I. Szlufarska, and D. Morgan, Acta Mater. **91**, 340 (2015).

[61] M. Alinger, S. Glade, B. Wirth, G. Odette, T. Toyama, Y. Nagai, and M. Hasegawa, Mater. Sci. Eng. A **518**, 150 (2009).

[62] V. Krsjak, Z. Szaraz, and P. Hähner, J. Nucl. Mater. **428**, 160 (2012).

[63] S. Moll, T. Jourdan, and H. Lefaix-Jeuland, Phys. Rev. Lett. **111**, 015503 (2013).

[64] C. Flynn, *Point Defects and Diffusion, International Series of Monographs on Physics* (Oxford University Press, New York, 1972).